Article

Cell Reports

An Unusual Prohibitin Regulates Malaria Parasite Mitochondrial Membrane Potential

Graphical Abstract

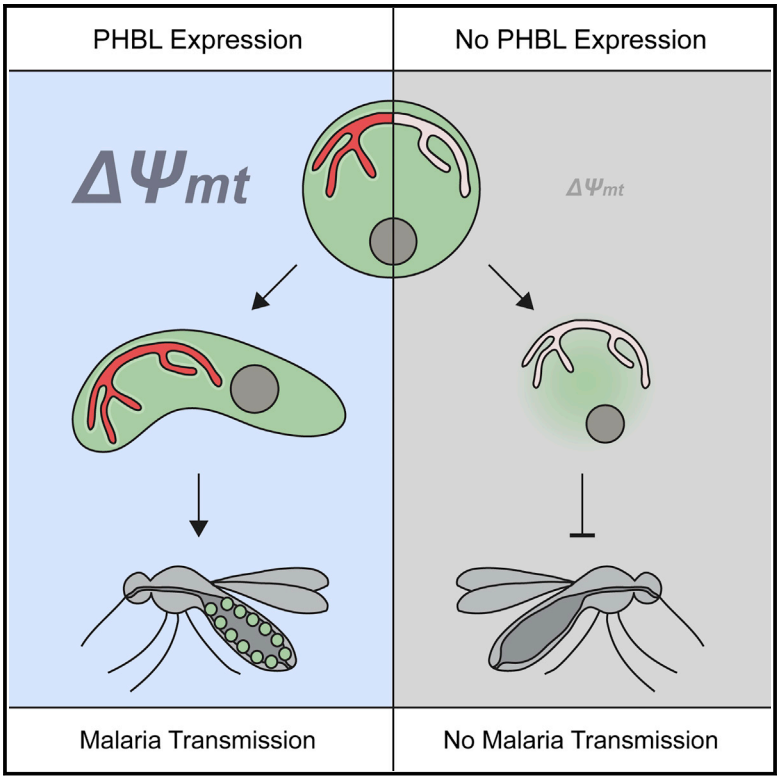

Highlights

- *Plasmodium* encodes three conserved SPFH proteins and one unusual family member, PHBL
- PHBL is a Myzozoa-specific protein that promotes development in the mammalian host
- PHBL function is essential for parasite colonization of the mosquito vector
- PHBL-dependent transmission arrest correlates with the loss of $\Delta\Psi_{mt}$

Authors

Joachim Michael Matz, Christian Goosmann, Kai Matuschewski, Taco Wilhelmus Antonius Kooij

Correspondence

joachim.michael.matz@hu-berlin.de (J.M.M.), taco.kooij@radboudumc.nl (T.W.A.K.)

In Brief

Matz et al. present an experimental genetics study of an unusual prohibitin-like protein in the malaria parasite and find that it regulates mitochondrial membrane polarity. Ablation of this protein causes almost complete mitochondrial depolarization in the mosquito vector, which, in turn, leads to a block in malaria parasite transmission.

Matz et al., 2018, Cell Reports *23*, 756–767
April 17, 2018
https://doi.org/10.1016/j.celrep.2018.03.088

CellPress

OPEN ACCESS
CellPress

Cell Reports
Article

An Unusual Prohibitin Regulates Malaria Parasite Mitochondrial Membrane Potential

Joachim Michael Matz,[1,2,3,6,*] Christian Goosmann,[4] Kai Matuschewski,[1,2] and Taco Wilhelmus Antonius Kooij[3,5,*]
[1]Department of Molecular Parasitology, Institute of Biology, Humboldt University, Philippstraße 13, 10115 Berlin, Germany
[2]Parasitology Unit, Max Planck Institute for Infection Biology, Charitéplatz 1, 10117 Berlin, Germany
[3]Department of Medical Microbiology, Radboud Institute for Molecular Life Sciences, Radboud University Medical Center, PO Box 9101, 6500 HB Nijmegen, the Netherlands
[4]Microscopy Core Facility, Max Planck Institute for Infection Biology, Charitéplatz 1, 10117 Berlin, Germany
[5]Center for Molecular and Biomolecular Informatics and Radboud Center for Mitochondrial Medicine, Radboud Institute for Molecular Life Sciences, Radboud University Medical Center, PO Box 9101, 6500 HB Nijmegen, the Netherlands
[6]Lead Contact
*Correspondence: joachim.michael.matz@hu-berlin.de (J.M.M.), taco.kooij@radboudumc.nl (T.W.A.K.)
https://doi.org/10.1016/j.celrep.2018.03.088

SUMMARY

Proteins of the stomatin/prohibitin/flotillin/HflK/C (SPFH) family are membrane-anchored and perform diverse cellular functions in different organelles. Here, we investigate the SPFH proteins of the murine malaria model parasite *Plasmodium berghei*, the conserved prohibitin 1, prohibitin 2, and stomatin-like protein and an unusual prohibitin-like protein (PHBL). The SPFH proteins localize to the parasite mitochondrion. While the conserved family members could not be deleted from the *Plasmodium* genome, *PHBL* was successfully ablated, resulting in impaired parasite fitness and attenuated virulence in the mammalian host. Strikingly, *PHBL*-deficient parasites fail to colonize the *Anopheles* vector because of complete arrest during ookinete development *in vivo*. We show that this arrest correlates with depolarization of the mitochondrial membrane potential ($\Delta\Psi_{mt}$). Our results underline the importance of SPFH proteins in the regulation of core mitochondrial functions and suggest that fine-tuning of $\Delta\Psi_{mt}$ in malarial parasites is critical for colonization of the definitive host.

INTRODUCTION

Proteins containing the stomatin/prohibitin/flotillin/HflK/C (SPFH) domain can be found all across prokaryotic and eukaryotic life. Members of this protein family comprise stomatin, stomatin-like proteins (SLPs), prohibitins, flotillins, podocin, erlins, and a multitude of bacterial membrane proteins (Browman et al., 2007). Whether the SPFH domain evolved independently in different proteins or whether the SPFH family members share a common ancestry remains a matter of debate (Rivera-Milla et al., 2006; Hinderhofer et al., 2009).

SPFH proteins share the ~185-amino acid SPFH domain and contain at least one hydrophobic amino acid stretch, which promotes association with detergent-resistant membranes of various organelles, where they form large protein complexes of 12 or more monomers (Morrow and Parton, 2005; Browman et al., 2007).

Cumulating evidence suggests that SPFH protein complexes perform scaffolding functions for proteins and lipids and serve as molecular platforms for a multitude of cellular processes (Langhorst et al., 2005; Osman et al., 2009). For instance, the mitochondrial prohibitin complex has been linked to protein degradation, mitochondrial morphogenesis, apoptosis, membrane organization, assembly of the respiratory chain, and maintenance of mitochondrial DNA (Osman et al., 2009; Merkwirth and Langer, 2009). This enormous diversity is indicative of a general propensity of SPFH proteins to compartmentalize membranes and sequester diverse proteins and catalytic activities.

The remarkable versatility of SPFH complexes prompted us to investigate this protein family in a parasitic single-cell eukaryote that faces very different host environments throughout a highly complex life cycle. Malaria parasites infect a variety of tissues, including the blood and liver of a mammalian host and the midgut, hemocoel, and salivary glands of a mosquito vector. SPFH protein complexes might therefore be key players promoting critical adaptations during these different life cycle stages.

To reveal their subcellular localizations and physiological roles, we performed experimental genetics in the murine model parasite *Plasmodium berghei* and reveal distinct functions of an unusual prohibitin-like protein in the regulation of the mitochondrial membrane potential during host switching.

RESULTS

SPFH Proteins of the Malaria Parasite

We initiated our analysis with a systematic database search for *Plasmodium* SPFH proteins and uncovered four candidates that either display a close phylogenetic relationship to conserved members—prohibitin 1 (PHB1, PBANKA_0701500), prohibitin 2 (PHB2, PBANKA_1213100), and stomatin-like protein (STOML, PBANKA_0807100)—or fall into a unique sister group that contains related proteins from the phylum Myzozoa, which harbors the subphylum Apicomplexa (Figure 1A). Accordingly, we named the latter *Plasmodium* protein prohibitin-like protein (PHBL, PBANKA_0718600). All four proteins contain a central signature

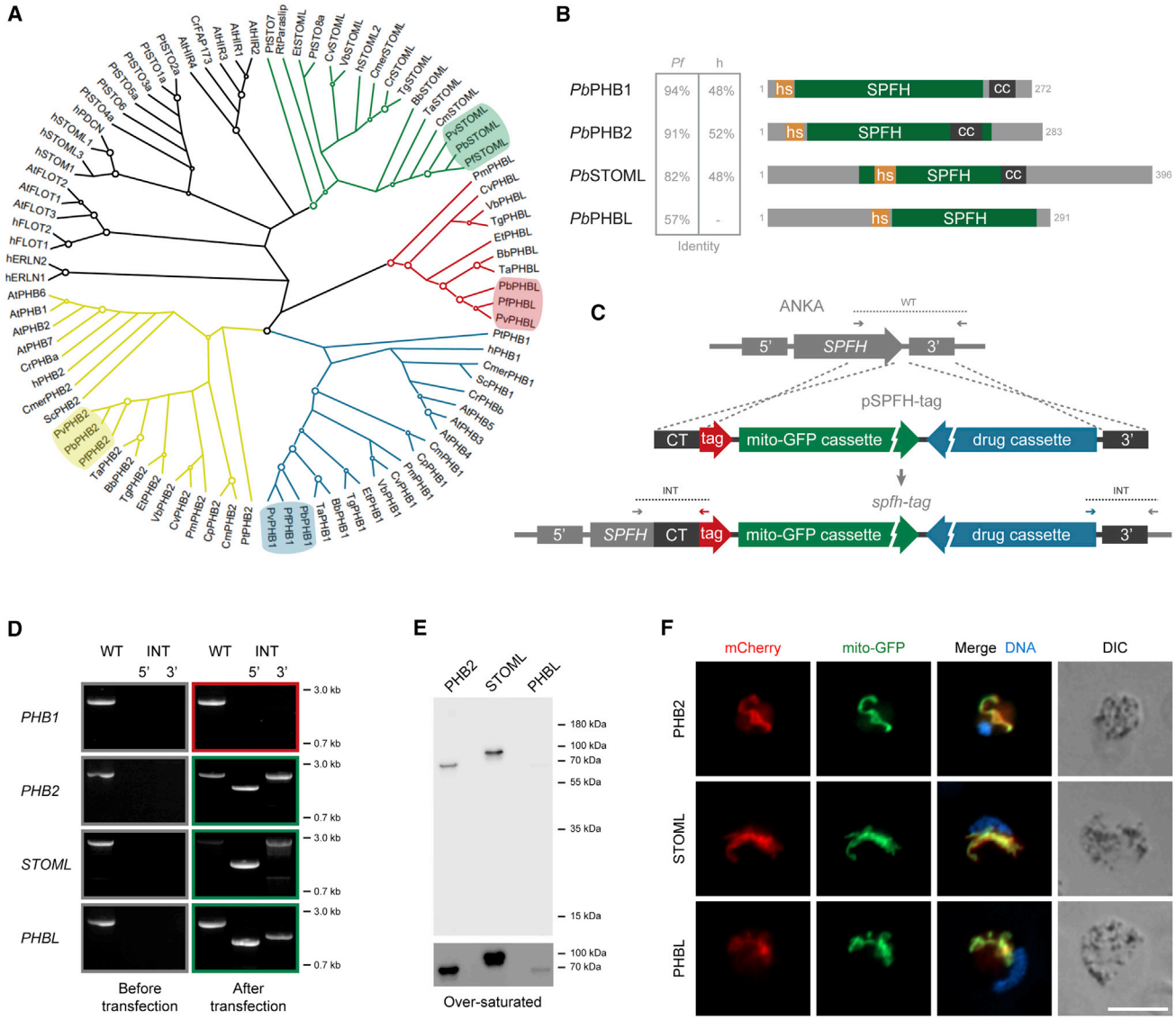

Figure 1. *Plasmodium berghei* SPFH Proteins Localize to the Parasite Mitochondrion

(A) Phylogenetic analysis demonstrates the presence of canonical prohibitin 1 (PHB1, blue) and 2 (PHB2, yellow), a single stomatin-like protein (STOML, green), and a prohibitin-like protein (PHBL, red) unique to Myzozoa in *Plasmodium*. Shown is a maximum likelihood tree of 89 SPFH proteins from apicomplexan parasites, related alveolates, representative eukaryotic species, and a prokaryote (Supplemental Experimental Procedures). Big circles, nodes with bootstrap values of more than 90%; small circles, nodes with values of 65%–90%. *Plasmodium* proteins are highlighted.

(B) Domain architecture and conservation of the plasmodial SPFH proteins. The table indicates the identity values of the *P. berghei* SPFH protein sequences with the *P. falciparum* (*Pf*) and human (h) homologs. hs, hydrophobic stretch; SPFH, SPFH domain; cc, coiled coil; gray numbers, start and end of the amino acid sequence.

(C) Replacement strategy for the generation of stable parasite lines expressing the endogenous *Plasmodium* SPFH proteins PHB1 or PHBL (*SPFH*) fused to mCherry-3xMyc (tag). Recombinant parasites contain the drug-selectable hDHFR-yFcu cassette (drug cassette) and a mitochondrial marker cassette consisting of the promoter and N terminus of *HSP70-3* (PBANKA_0914400) fused to GFP (mito-GFP; see also Figure S1A). CT, C terminus. Wild-type (WT)-specific and integration (INT)-specific primer combinations are indicated by arrows and expected fragments by dotted lines. Note that endogenous tagging of *PHB2* and *STOML* was performed by single homologous recombination (see also Figure S1B).

(D) Diagnostic PCR of genomic DNA from parasites before (left) and after transfection (right) using the primer combinations shown in (C). Green frames denote successful endogenous tagging. The red frame indicates that three independent transfection experiments did not result in the recovery of the desired *phb1-tag* parasite line.

(E) Western blot analysis of transgenic parasites expressing tagged SPFH proteins using anti-mCherry antibodies. Predicted molecular weights: PHB2-tag, 64.5 kDa; STOML-tag, 77.5 kDa; PHBL-tag, 68.4 kDa. The blot has been over-saturated for enhanced visibility of tagged PHBL (bottom).

(F) Immunofluorescence analysis of transgenic blood stage parasites using anti-mCherry and anti-GFP antibodies. Depicted are representative micrographs of the tagged proteins (red, left), the mito-GFP marker (green, center left), a merge of both signals with Hoechst 33342 nuclear dye (DNA, blue, center right), and differential interference contrast images (DIC, right). Scale bar, 5 μm.

SPFH domain and a hydrophobic stretch (Figure 1B). Although the conventional *Plasmodium* SPFH proteins display a similarly high degree of conservation, PHBL sequences are rather divergent already among related *Plasmodium* species (Figure 1B).

PHB2, STOML, and PHBL Localize to the Malaria Parasite Mitochondrion

Because SPFH proteins are known to localize to the membranes of several different organelles, we first wanted to analyze their subcellular distribution in malaria parasites. To that end, we generated transgenic *P. berghei* lines expressing the endogenous SPFH proteins fused to an mCherry-3xMyc tag. In addition, transfection vectors contained the mitochondrial marker cassette mito-GFP for protein co-localization (Figures 1C, S1A, and S1B).

We successfully generated transgenic lines expressing tagged PHB2, STOML, and PHBL (Figure 1D). In contrast, repeated transfection experiments did not result in the recovery of a transgenic line expressing tagged PHB1, suggesting that perturbation of the locus is lethal to the parasite (Figure 1D). Western blot analysis of parasite extracts confirmed the presence of full-length PHB2, STOML, and PHBL fusion proteins and provided no evidence for processing or degradation (Figure 1E). The expression of PHBL appeared to be much lower than the expression of PHB2 and STOML. Therefore, we employed immunofluorescence analysis of the transgenic blood stage parasites using anti-mCherry and anti-GFP antibodies to enhance the signals of the tagged proteins. Co-localization with the mito-GFP marker revealed that PHB2, STOML, and PHBL all localize to the parasite mitochondrion (Figure 1F).

Next we analyzed the expression of SPFH proteins during the remaining life cycle stages. Live fluorescence microscopy of the *phb2-tag*, *stoml-tag*, and *phbl-tag* lines demonstrated ubiquitous expression of all three proteins during parasite development in the vertebrate and mosquito hosts (Figure 2). PHBL displayed very low expression levels throughout development and was undetectable in young ring stages (Figure 2C). Interestingly, STOML was found to concentrate at punctate foci of the parasite mitochondrion during oocyst growth, often at organellar branching points (Figure 2B).

Plasmodium berghei PHBL Is Dispensable for Blood Infection

To assess the importance of the SPFH proteins during asexual blood propagation, we attempted to delete the corresponding genes from the *P. berghei* genome (Figure 3A). Three attempts to ablate *PHB1*, *PHB2*, and *STOML* did not result in the recovery of gene deletion mutants, hinting at essential functions during asexual blood stage development (Figure 3B). The successful selection of endogenously labeled *phb2-tag* and *stoml-tag* parasite lines (Figure 1D) supports the notion that the corresponding loci are accessible to genetic manipulation, signifying incompatibility of the absence of *PHB2* or *STOML* with parasite propagation during blood infection.

In contrast, we were able to isolate transgenic mCherry-fluorescent parasites that lack expression of *PHBL* using flow cytometry (Kenthirapalan et al., 2012). Correct genomic integration in the isogenic parasite line was confirmed by diagnostic PCR and Southern blot analysis (Figures 3B and S1G). We tested the performance of the *phbl*$^{-}$ parasites during asexual blood stage development employing an intravital competition assay (Matz et al., 2013). Strikingly, the *PHBL*-deficient mutant grew at only 37% of the wild-type (WT) rate (Figure 3C). 7 days after co-injection of the WT and mutant, only 1% of all blood stage parasites were *phbl*$^{-}$, highlighting the marked fitness disadvantage in the absence of *PHBL*. As a consequence, *phbl*$^{-}$ parasites showed attenuated virulence, and infected mice did not succumb to experimental cerebral malaria (Figure 3D).

phbl^{-} Parasites Fail to Transmit

The ubiquitous expression of *PHBL* prompted us to test the performance of *phbl*$^{-}$ parasites during life cycle progression. Therefore, we fed highly infected mice to female *Anopheles stephensi* mosquitoes. Because of the prominent blood stage propagation defect, we injected a 4-fold higher *phbl*$^{-}$ inoculum in comparison to WT parasites, resulting in comparable parasitemias on days 3 and 4 after injection (Figure S2). On day 21 after the blood meal, infected mosquitoes were allowed to feed on naive C57BL/6 mice, and peripheral blood was monitored daily by microscopic examination of Giemsa-stained thin blood films. As expected, all animals bitten by WT-infected mosquitoes became blood stage-positive on day 3 after bite back (Figure 4A). In stark contrast, transmission of *phbl*$^{-}$ parasites was completely abolished. Not a single mouse that had received bites from mosquitoes infected with *phbl*$^{-}$ parasites developed a patent blood infection, demonstrating essential functions of *PHBL* for life cycle progression (Figure 4A).

We next wanted to determine the exact timing of the developmental arrest and tested the capacity of *PHBL*-deficient parasites to form gametocytes. Analysis of peripheral blood revealed comparable gametocyte conversion rates on days 3 and 4 after injection (Figure 4B). In agreement with this, *phbl*$^{-}$ parasites displayed normal exflagellation behavior (Figure 4C).

PHBL Is Essential for Ookinete Development *In Vivo*

To test the fertility of *PHBL*-deficient gametocytes, we inoculated *in vitro* cultures with highly infected blood and quantified the formation of ookinetes. To that end, cultures were stained with an antibody directed against P28, a surface antigen of macrogametes, zygotes, and ookinetes (Sinden et al., 1987). Live-cell imaging revealed that 38% of P28-positive WT parasites had developed into mature ookinetes (Figures 4D and 4E). In contrast, only 7% of the *phbl*$^{-}$ parasites reached this developmental stage (Figures 4D and 4E). An additional clonal *phbl*$^{-}$ line formed similarly low numbers of ookinetes (Figure S6B). *phbl*$^{-}$ ookinetes were viable; they displayed normal gliding motility in Matrigel (Video S1).

The impairment of ookinete formation *in vitro* prompted us to further explore sexual parasite development in the invertebrate host. To that end, female *A. stephensi* mosquitoes were fed on highly infected mice, and mosquito midguts were removed 18 hr later. P28 labeling of the ingested blood revealed that 4% of WT macrogametes had developed into ookinetes (Figures 4D and 4F). Strikingly, no ookinetes were observed in the blood meals of mosquitoes fed with *phbl*$^{-}$-infected mice (Figures 4D and 4F). Instead, P28-positive *phbl*$^{-}$ parasites displayed an

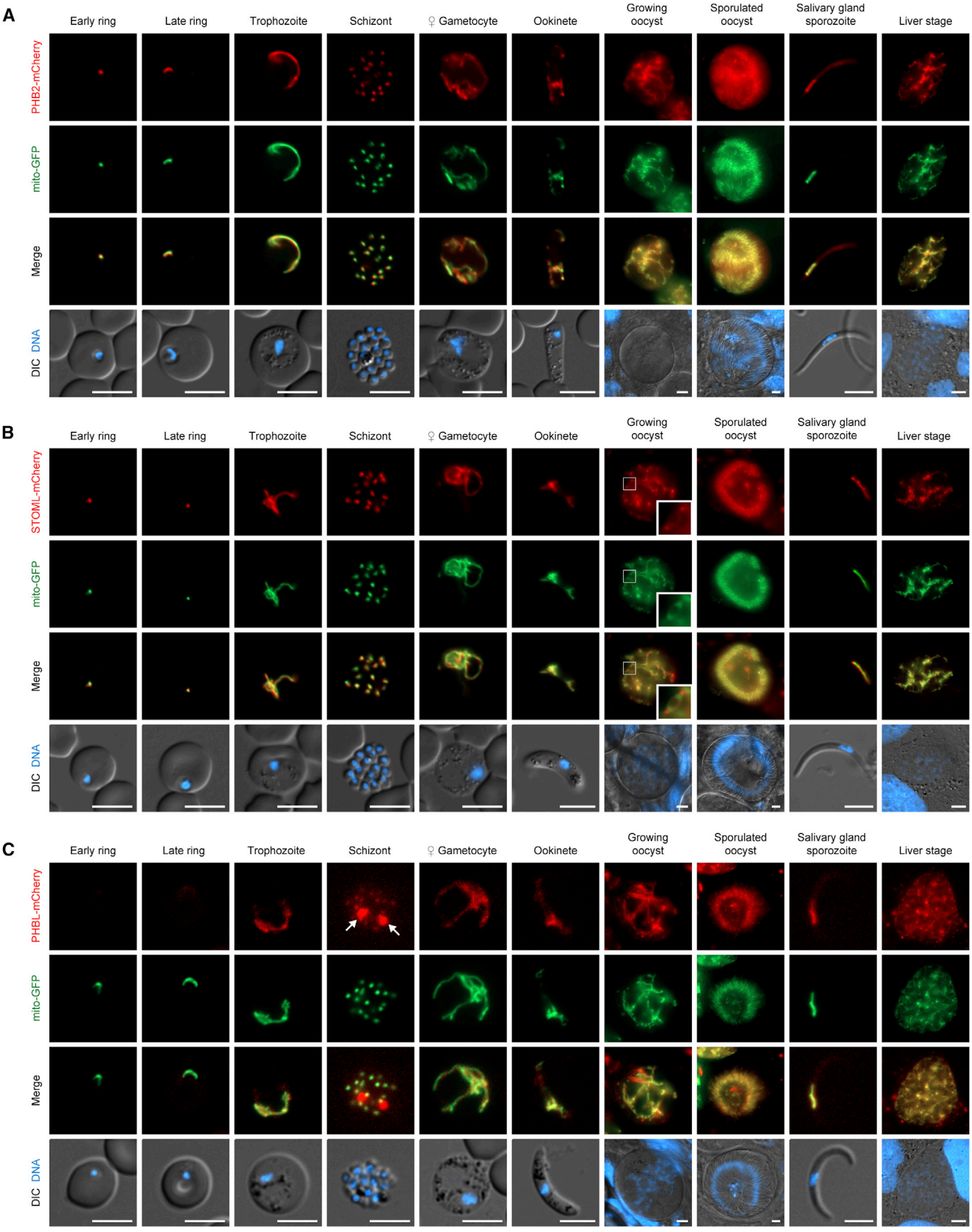

(legend on next page)

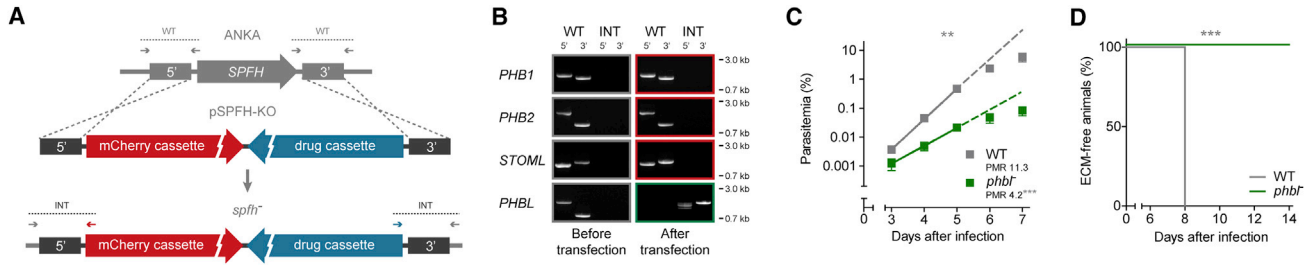

Figure 3. Systematic Gene Targeting Reveals Important Functions of SPFH Proteins during Asexual Blood Stage Development

(A) Replacement strategy to delete the four genes encoding the SPFH proteins of *Plasmodium berghei*. The respective loci (*SPFH*) were targeted with replacement plasmids containing 5′ and 3′ regions flanking the open reading frames, an expression cassette for high-level cytoplasmic mCherry fluorescence, and the drug-selectable hDHFR-yFcu cassette (drug cassette). WT-specific and INT-specific primer combinations are indicated by arrows and expected fragments by dotted lines.

(B) For each target gene, diagnostic PCRs of the WT locus (left) and of the drug-selected and isolated parasites (right) are shown, using the primer combinations shown in (A). The green frame denotes successful isolation of the *PHBL* loss-of-function mutant. Red frames indicate that three or more independent transfection experiments did not result in recovery of a gene deletion strain. Note that a second independent *PHBL* loss-of-function mutant expressing mito-GFP has been isolated (see also Figures S1E–S1G).

(C) Intravital competition assay demonstrates a large blood propagation defect of the *phbl*⁻ line. 500 GFP-fluorescent Bergreen WT and 500 mCherry-fluorescent *phbl*⁻ blood stage parasites were co-injected into naive NMRI mice, and peripheral blood was analyzed daily by flow cytometry. Mean values (± SD) are shown for each time point. **p < 0.01, two-way ANOVA; ***p < 0.001; PMR, parasite multiplication rate; n = 3.

(D) Kaplan-Meier analysis of time to development of signature experimental cerebral malaria (ECM) symptoms. C57BL/6 mice were injected intravenously with 1,000 Bergreen WT or *phbl*⁻ blood stage parasites. ***p < 0.001, Mantel-Cox test, n = 5.

aberrant morphology and decreased size (Figure 4D). During several experiments, no P28-positive *phbl*⁻ parasites were detected in the blood meal, despite prominent gametocytemia in the donor mice and ookinete formation *in vitro*, suggesting rapid mortality of early sexual stages and subsequent parasite disintegration *in vivo*.

To exclude a specific *PHBL*-dependent *in vivo* fertilization defect, we fed highly infected mice to mosquitoes and subsequently transferred the ingested blood to *in vitro* cultures. During three independent experiments, both WT and *phbl*⁻ ookinetes were detected after 2 hr of midgut exposure and subsequent cultivation, confirming successful fertilization *in vivo* (Figure 5A). While approximately 11% of WT macrogametes had transformed into mature ookinetes, *phbl*⁻ ookinete numbers were too low for confident quantification, reinforcing that *phbl*⁻ parasite mortality occurs early after blood ingestion.

Transmission electron microscopy revealed that arrested *phbl*⁻ parasites are much more electron-lucent than ookinetes recovered from WT-infected mosquitoes, indicative of partial parasite lysis or leakage (Figures 5B and 5D). Indeed, the morphology of *phbl*⁻ parasites was similar to that of WT parasites arrested during early ookinete development (Figure 5C). This includes the formation of an electron-dense pellicular region, the progenitor of the apical complex (Figures 5C–5E). The mitochondrion of the arrested *phbl*⁻ parasites appeared to be intact and displayed a similar morphology as in arrested WT parasites (Figures 5B–5D).

Together with the detection of successful albeit 5-fold reduced formation of *phbl*⁻ ookinetes *in vitro*, these data suggest that *PHBL* is not essential for fertilization but, rather, promotes survival during mosquito midgut colonization. Inspection of the midgut wall 24 hr after feeding confirmed that WT ookinetes had traversed the epithelium, whereas *phbl*⁻ parasites were completely absent (Figure 4G). As a consequence, no *PHBL*-deficient oocysts or sporozoites were observed (Figures 4H–4J).

Mitochondrial Organization of *PHBL*-Deficient Parasites Remains Unaltered

Depletion of prohibitins has been shown to interfere with mitochondrial morphogenesis in yeast (Piper et al., 2002) and several metazoan species (Artal-Sanz et al., 2003; Kasashima et al., 2006; Merkwirth et al., 2008). Therefore, we tested whether the prominent fitness cost in the absence of *PHBL* is associated with aberrant mitochondrial morphogenesis. We generated and isolated mutant parasites expressing fluorescent mitochondrial marker proteins in the presence or absence of *PHBL*. Live fluorescence microscopy of the generated $WT_{mito\text{-}mCh}$ reference line (Figures S1C and S1D) revealed the typical dot-like pattern in young ring stages, the rod-like morphology during parasite growth, the branching, and, ultimately, the organellar division during the schizont stage (Figure S3A; van Dooren et al., 2005). A second independent gene deletion line expressing mito-GFP was generated to analyze mitochondrial morphology in the absence of *PHBL* (Figures S1E–S1G). Live-cell imaging of the

Figure 2. SPFH Proteins Are Expressed throughout the Entire *Plasmodium* Life Cycle

(A–C) *phb2-tag* (A), *stoml-tag* (B), and *phbl-tag* (C) parasites were imaged live at different life cycle stages. Shown are representative images, including the fluorescent signals of the mCherry-3xMyc-tagged SPFH proteins (red, first row), the mito-GFP marker (green, second row; see also Figure S1A), a merge of both signals (third row), and a merge of DIC images with Hoechst 33342 nuclear dye (DNA, blue, fourth row). A mitochondrial section of a growing *stoml-tag* oocyst is depicted in an inset. Arrows indicate autofluorescence of hemozoin-containing digestive vacuoles, which was also observed in WT schizonts, because of prolonged exposure times. Scale bars, 5 μm.

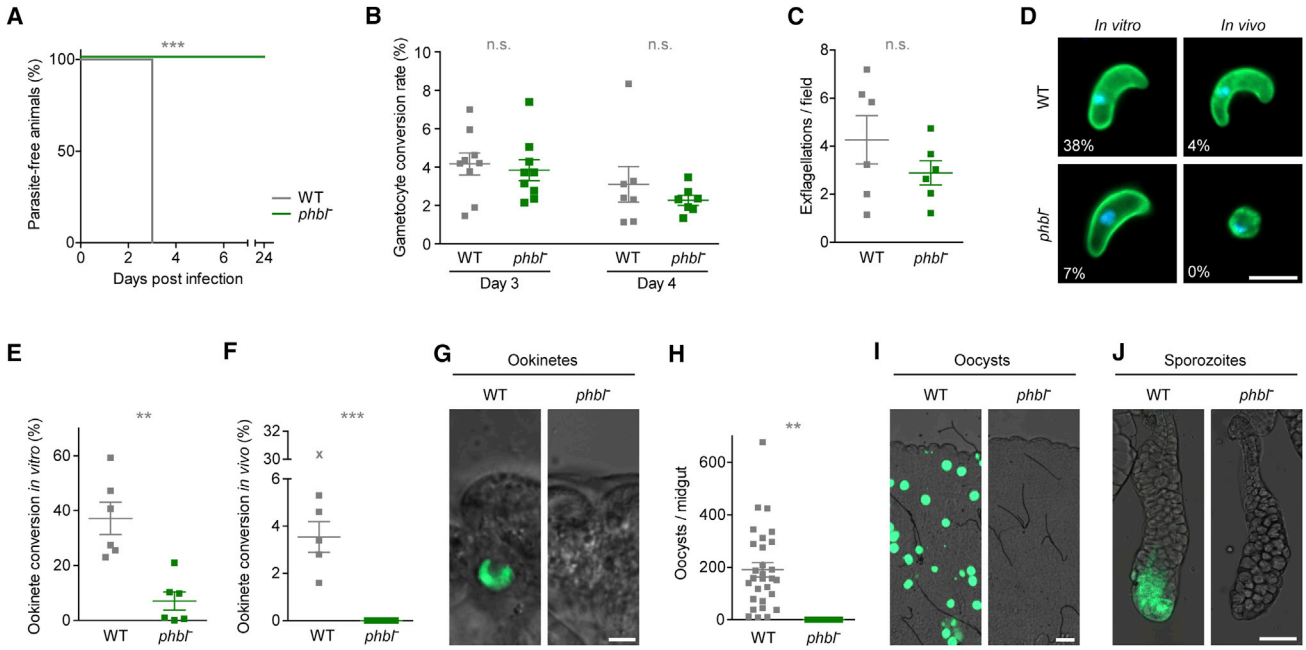

Figure 4. *PHBL*-Deficient Parasites Fail to Transmit

(A) Kaplan-Meier analysis of time to development of patent blood stage infection. Naive C57BL/6 mice were subjected to bites by mosquitoes that received blood meals of mice infected with Bergreen WT or *phbl*⁻ parasites and were monitored daily by microscopic analysis of Giemsa-stained thin blood films. ***$p < 0.001$, Mantel-Cox test, n = 12 mice from 3 independent bite back experiments.

(B) Gametocyte production 3 and 4 days after intravenous injection of Bergreen WT or *phbl*⁻ parasites, as determined by Giemsa-stained thin blood films. The gametocyte conversion rate was calculated as the percentage of all blood stages. Shown are the mean values (± SEM). n.s., non-significant; Student's t test, n = 7.

(C) Quantification of exflagellation centers by microscopic analysis of peripheral blood 3 days after intravenous injection of Bergreen WT or *phbl*⁻ parasites. The inoculum was different for WT (1×10^7) and *phbl*⁻ (4×10^7) parasites to achieve comparable parasitemias on days 3 and 4 after injection (see also Figure S2). Shown are the mean values (± SEM). Student's t test, n = 6.

(D) Representative live fluorescence micrographs of Berred WT (top) and *phbl*⁻ ookinetes (bottom) from *in vitro* culture (left) or from mosquito midguts (right). Parasites were stained with a primary anti-P28 antibody and a fluorescently labeled secondary antibody. Depicted is a merge of the P28 signal (green) and Hoechst 33342 nuclear dye (DNA, blue). Numbers indicate the percentage of ookinetes among P28-positive parasites. Scale bar, 5 μm. For ookinete gliding, see Video S1.

(E and F) Ookinete conversion is significantly reduced *in vitro* (E) and completely abrogated *in vivo* (F). Ookinete conversion was calculated as the percentage of P28-positive parasites. Shown are the mean values (± SEM). **$p < 0.01$, ***$p < 0.001$, Student's t test, n = 6. The gray X marks an unusually high value that was treated as an outlier. $p < 0.05$; Grubbs' test for outliers. For a comparison between *in vitro* ookinete conversion of isogenic and clonal *phbl*⁻ parasites, see Figure S6B.

(G) Representative micrographs of mosquito midguts after removal of the blood boli, extracted 24 hr after the infectious blood meals. Shown is a merge of the parasite's cytoplasmic fluorescence (Bergreen WT, green; *phbl*⁻, red) and DIC images. Scale bar, 5 μm.

(H) Quantification of midgut-associated Bergreen WT and *phbl*⁻ oocysts 10 days after the infectious blood meals. Shown are the mean values (±SEM). **$p < 0.01$, Student's t test, n = 30 midguts from 3 independent experiments.

(I and J) Representative micrographs of (I) mosquito midguts 10 days and (J) salivary glands 21 days after infectious blood meals. Shown is a merge of the parasite's cytoplasmic fluorescence (Bergreen WT, green; *phbl*⁻, red) and DIC images. Scale bars, 50 μm.

resultant $phbl^-_{mito\text{-}GFP}$ parasites did not reveal any differences in mitochondrial morphology or integrity during the asexual blood cycle compared with $WT_{mito\text{-}mCh}$ (Figure S3A). Also, organellar division appeared to be normal because all observed merozoites harbored a single GFP-fluorescent mitochondrion.

We then purified WT and *phbl*⁻ macrogametes to assess their ultrastructure by transmission electron microscopy. PHBL-deficient mitochondria displayed a similar degree of complexity as WT mitochondria (Figure S3B). Quantification of the area occupied by the parasite mitochondrion and of the mitochondrial aspect ratios supports the notion of normal mitochondrial size and integrity in *phbl*⁻ macrogametes (Figures S3C and S3D). Furthermore, arrested *phbl*⁻ parasites extracted from mosquito midguts displayed a similar mitochondrial morphology as WT parasites (Figures 5B–5D). To validate this further, purified $WT_{mito\text{-}mCh}$ and $phbl^-_{mito\text{-}GFP}$ macrogametes were imaged using live fluorescence microscopy. Interestingly, $phbl^-_{mito\text{-}GFP}$ gametocytes or exflagellation events were observed only rarely in peripheral blood (Figures S3E and S3F). Because gametocytogenesis of the $WT_{mito\text{-}mCh}$ reference strain and the *phbl*⁻ line expressing cytoplasmic mCherry were not impaired (Figures 4B, 4C, S3E, and S3F), we reason that the import of mito-GFP exerts additional stress on the already dysfunctional PHBL-deficient mitochondrion, leading to added fitness loss in developing

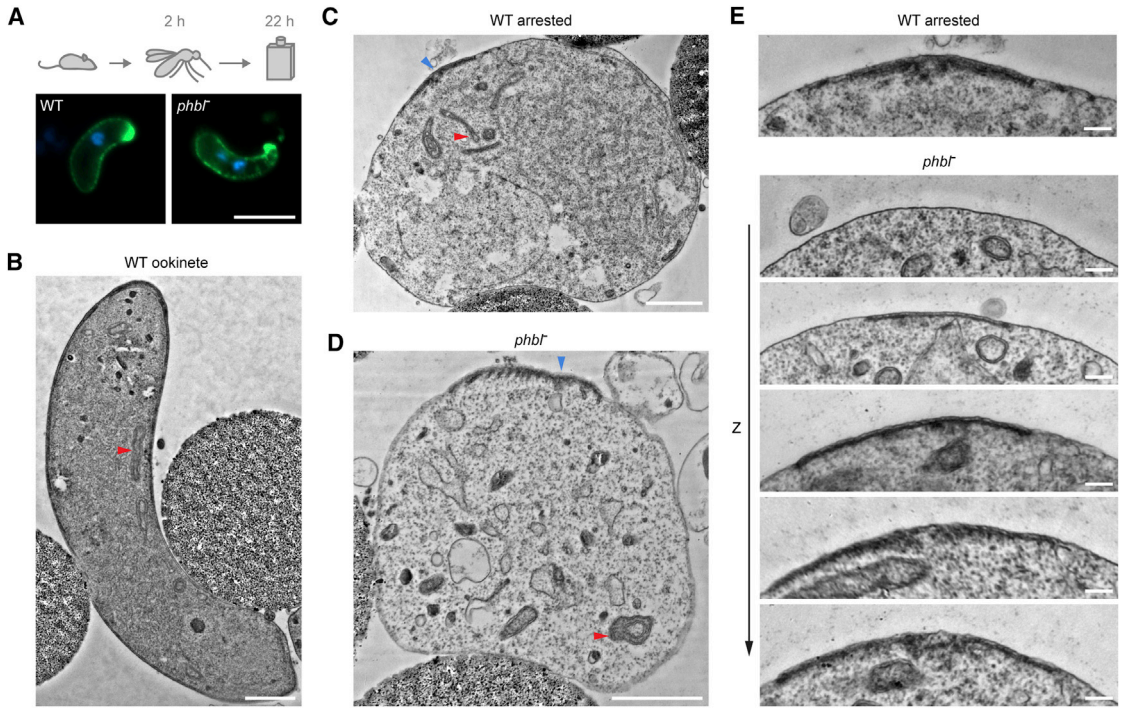

Figure 5. *PHBL*-Deficient Parasites Arrest Early after Fertilization

(A) Fertilization of *phbl*⁻ gametes occurs *in vivo*. Female *Anopheles stephensi* mosquitoes were allowed to feed on highly infected mice. 2 hr after the bite, the ingested blood was transferred to *in vitro* culture for 22 hr. Representative micrographs of formed WT and *phbl*⁻ ookinetes are shown as a merge of the P28 signal (green) and Hoechst 33342 nuclear dye (DNA, blue). Scale bar, 5 μm.

(B–D) Transmission electron micrographs of WT and *phbl*⁻ parasites during the time of transmission. Mosquitoes were allowed to feed on highly infected mice. 18 hr after the meal, blood boli were removed and subjected to P28 affinity purification, thus enriching sexually differentiated parasite stages. Shown is a WT ookinete (B), a WT parasite arrested during sexual development (C), and a purified *phbl*⁻ parasite (D). Red arrowheads, parasite mitochondria; blue arrowheads, electron-dense regions of the parasite pellicle, indicative of apical complex biogenesis. The spherical structures adjacent to the parasites are magnetic beads used for affinity purification. Scale bars, 1 μm. For a comparison of mitochondrial morphology, see Figure S3.

(E) Intermediates of the apical complex in arrested WT (top) and *phbl*⁻ (bottom) parasites. Consecutive transmission electron microscopic sections are shown for one *phbl*⁻ parasite (Z). Scale bars, 0.2 μm.

phbl$^{-}_{\text{mito-GFP}}$ gametocytes. Nonetheless, macrogametes could be enriched using anti-P28 antibody-labeled magnetic beads, and both WT$_{\text{mito-mCh}}$ and *phbl*$^{-}_{\text{mito-GFP}}$ parasites showed the typical highly structured mitochondrial morphology of sexual stage parasites (Figure S3G).

PHBL Supports Efficient Mosquito-Mouse Transition

To test whether liver stage development was also impaired by the loss of *PHBL*, we rescued the mosquito stage arrest by cross-fertilizing the mCherry-fluorescent *phbl*⁻ parasites with GFP-fluorescent Bergreen WT parasites *in vivo*. A dually infected donor mouse was fed to *A. stephensi* mosquitoes after confirming the presence of both parasite populations by flow cytometry (Figure 6A). Fluorescence microscopy of mosquito midguts revealed that all mCherry-positive oocysts carrying the *phbl*⁻ allele were also expressing GFP, confirming successful cross-fertilization and phenotypic rescue (Figure 6B).

After 21 days, infected mosquitoes were allowed to transmit the parasites to naive C57BL/6 mice by bite. The fluorescent signals of both WT and *phbl*⁻ blood stage parasites were detected by flow cytometry 3 days after transmission (Figures 6C and 6D). As expected, a double-fluorescent parasite population lacking *PHBL* expression was detected as well because of the interchromosomal recombination events during mosquito-stage development (Figure 6C and genotype 4 in Figure S4). Diagnostic PCRs of parasite genomic DNA isolated from donor and recipient mice confirmed the presence of both WT and *phbl*⁻ alleles before and after transmission (Figure 6E).

Next we quantified host transition by comparing the percentages of the fluorescent sporozoite populations with the derived liver stages *in vitro* and the emerging blood stages *in vivo*. Although the morphology and quantity of *phbl*⁻ liver stages were normal *in vitro* (Figures 6F and 6G), the percentage of the *PHBL*-deficient emerging blood stage parasites *in vivo* was 9-fold lower than would be expected in the case of normal parasite fitness (Figure 6G).

These data argue for important but dispensable roles of *PHBL* during mosquito-mouse transition, which may be overcome by superior growth conditions in culture, as already demonstrated for ookinetes (Figures 4D–4F). Together with the detection of successful, albeit reduced, blood propagation, our findings underline the stage-specific essentiality of PHBL only during sexual

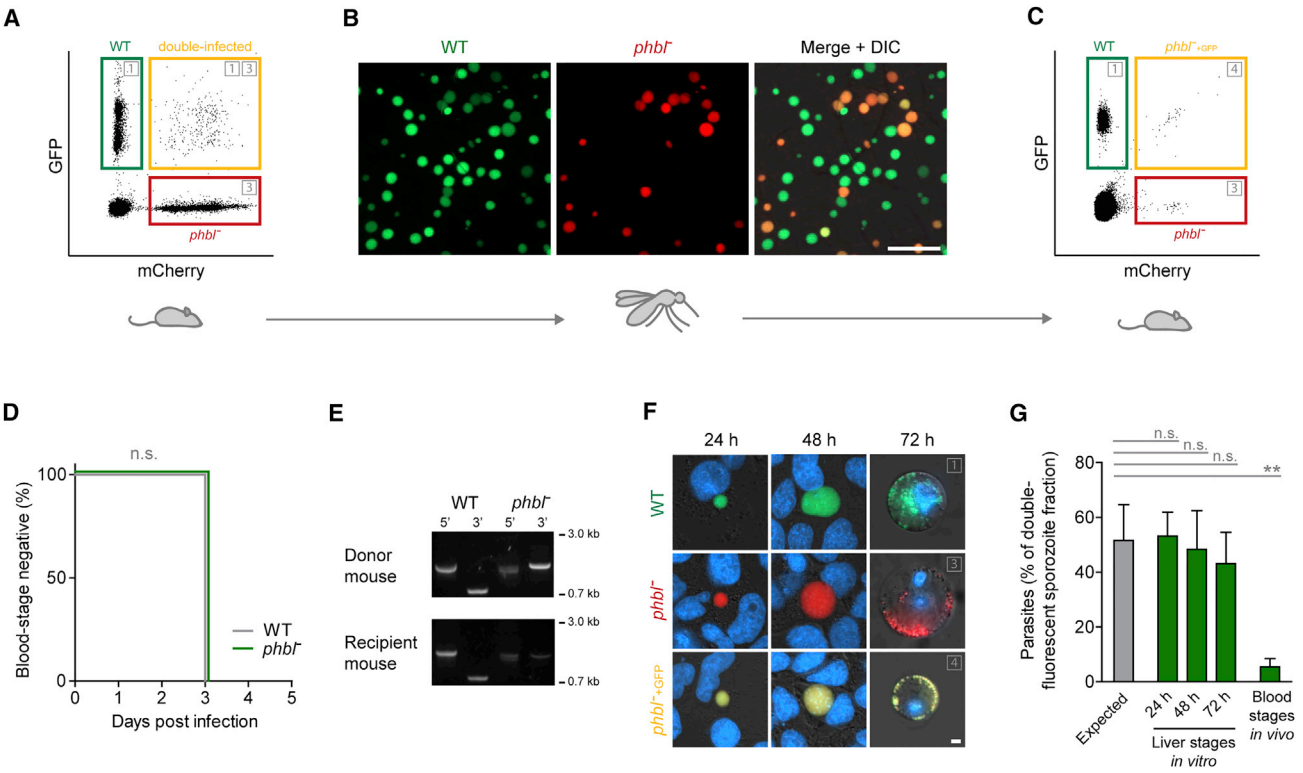

Figure 6. *PHBL* Supports Efficient Mosquito-Mouse Transition

NMRI mice were co-infected with both GFP-fluorescent Bergreen WT and mCherry-fluorescent *phbl*⁻ parasites, and female *Anopheles stephensi* mosquitoes were allowed to feed on infected mice, leading to cross-fertilization and phenotypic rescue during transmission. 21 days later, mosquitoes were allowed to feed on naive C57BL/6 mice.

(A) Flow cytometric detection of Bergreen WT and *phbl*⁻ parasites in the peripheral blood of a donor mouse. Double-fluorescent events represent erythrocytes harboring both WT and *phbl*⁻ parasites and are due to the high parasitemia prior to feeding (5%–10%). Boxed numbers indicate genotypes as depicted in Figure S4.

(B) Double-fluorescent oocysts confirm successful cross-fertilization. Depicted are the signals of the Bergreen WT-derived GFP (green), the *phbl*⁻-derived mCherry (red), and a merge with the DIC image. Note that no homozygous *phbl*⁻ oocysts (i.e., mCherry-positive and GFP-negative) were observed. Scale bar, 100 μm.

(C) Flow cytometric detection of Bergreen WT and *phbl*⁻ parasites in peripheral blood of a recipient mouse 3 days after sporozoite inoculation. Note that a *PHBL*-deficient double-fluorescent parasite population has emerged because of interchromosomal recombination events during development in the mosquito. Because of the low parasitemia (< 0.4%), double-infected erythrocytes, as shown in (A), do not occur yet. Boxed numbers indicate genotypes as depicted in Figure S4.

(D) Kaplan-Meier analysis of time to blood stage patency of the respective parasite populations upon bite back, as determined by flow cytometry. Mantel-Cox test, n = 6.

(E) Diagnostic PCR using genomic DNA from blood stage parasites isolated from a donor and a recipient mouse. WT-specific and knockout-specific primer combinations were used as shown in Figures 3A and 3B. Knockout-specific bands were detected in all recipient mice; n = 6.

(F) *In vitro* liver stage development of Bergreen WT and *PHBL*-deficient parasites. Shown are representative micrographs of liver stages 24 and 48 hr after invasion and detached cells 72 hr after invasion. The micrographs show a merge of the Bergreen WT-derived GFP (green), the *phbl*⁻-derived mCherry (red), Hoechst 33342 nuclear dye (blue), and DIC images. Scale bar, 5 μm. The occurrence of double-fluorescent parasites is due to interchromosomal recombination events during development in the mosquito and signifies the absence of *PHBL*. Boxed numbers indicate genotypes as depicted in Figure S4.

(G) Quantification of *PHBL*-deficient liver stages *in vitro* and emerging blood stages *in vivo* after inoculation with the mixed sporozoite population. Expected values reflect the fractions in the case of unaltered parasite fitness and are based on the percentage of observed double-fluorescent sporozoites. Shown are mean values (± SD). **p < 0.01, Student's t test, n = 3.

development and indicate important auxiliary roles in liver and blood infection.

PHBL Regulates Mitochondrial Membrane Potential during Sexual Development

Because of the precise and complete arrest of *phbl*⁻ parasites during colonization of the invertebrate host, we asked whether this striking developmental halt correlates with mitochondrial dysfunction during sexual differentiation. To that end, we measured the mitochondrial membrane potential ($\Delta\Psi_{mt}$) of WT and *phbl*⁻ mitochondria using the potentiometric dye rhodamine 123. Fluorescent mitochondria were observed in WT trophozoites, macrogametes, and *in vitro*-cultivated ookinetes (Figure 7A). As a negative control, WT parasites were treated with the

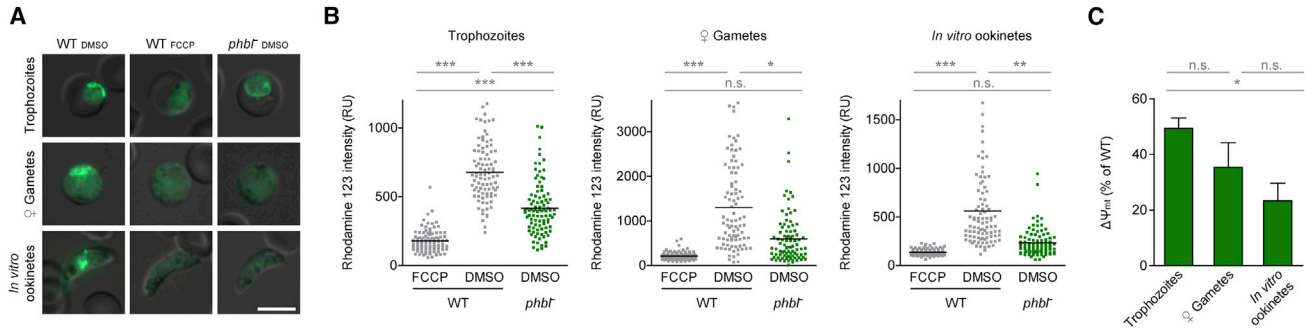

Figure 7. PHBL Regulates Mitochondrial Membrane Potential

Berred WT and *phbl*⁻ mitochondria were labeled with rhodamine 123, and the signal intensity was analyzed by live fluorescence microscopy. Carbonyl cyanide-4-(trifluoromethoxy)phenylhydrazone (FCCP) was used to uncouple $\Delta\Psi_{mt}$. In the absence of FCCP, DMSO served as the solvent control.

(A) Representative micrographs of blood stage trophozoites, macrogametes, and *in vitro*-cultivated ookinetes labeled with rhodamine 123 in the presence or absence of FCCP. Depicted is a merge of the fluorescent rhodamine 123 signal (green) and DIC images. Note, that FCCP treatment abolishes mitochondrial but not residual cytoplasmic rhodamine 123 labeling. Scale bar, 5 μm.

(B) Quantification of rhodamine 123 intensity by live fluorescence microscopy. Parasites were treated as described in (A). RU, relative units. Lines show mean values. *p < 0.05, **p < 0.01, ***p < 0.001, one-way ANOVA and Tukey's multiple comparison test using mean fluorescence values from the experimental replicates, n = 90 parasites from 6 independent experiments.

(C) $\Delta\Psi_{mt}$ in *PHBL*-deficient blood stage trophozoites, macrogametes, and *in vitro*-cultivated ookinetes, shown as percentage of WT. Values are derived from the rhodamine 123 intensities shown in (B) and were calculated as follows: $y = (phbl^{-}_{DMSO} - WT_{FCCP}) / (WT_{DMSO} - WT_{FCCP})$. Shown are mean values (± SD). *p < 0.05, one-way ANOVA and Tukey's multiple comparison test, n = 6.

For a comparison of FCCP-treated WT and *phbl*⁻ parasites, see Figure S5. For the quantification of atovaquone and oligomycin sensitivity, see Figures S6 and S7, respectively.

uncoupling agent carbonyl cyanide-4-(trifluoromethoxy)phenylhydrazone (FCCP), which resulted in complete loss of a mitochondrial signal during all stages (Figure 7A). WT and *phbl*⁻ parasites responded equally to FCCP treatment (Figure S5).

Staining of *PHBL*-deficient trophozoites with rhodamine 123 yielded a mitochondrial signal, albeit at lower intensities than in WT trophozoites (Figure 7A). Quantification of fluorescence intensities revealed that the mitochondrial staining of *phbl*⁻ trophozoites was reduced 2-fold (to 48%) in comparison with the WT signal (Figures 7B and 7C). This $\Delta\Psi_{mt}$ defect became more pronounced during sexual development; macrogametes showed only 35% of the WT membrane potential (Figures 7B and 7C), and *in vitro*-cultivated ookinetes revealed an almost completely depolarized parasite mitochondrion in the *phbl*⁻ strain. Although individual micrographs lacked a discernible mitochondrial signal and were indistinguishable from FCCP-treated WT samples (Figure 7A), quantification of the fluorescence intensities suggests that the $\Delta\Psi_{mt}$ of *phbl*⁻ ookinetes is decreased to 23% (Figures 7B and 7C). The degree of mitochondrial depolarization was significantly higher in ookinetes than in blood stage trophozoites. Despite the lack of statistical support, further comparison with macrogametes suggests a stepwise decrease of $\Delta\Psi_{mt}$ throughout sexual development (Figure 7C).

We found that this defect does not correlate with an altered sensitivity toward the complex III inhibitor and antimalarial drug atovaquone during asexual or sexual parasite development (Figures S6A and S6C). In agreement with this observation, exogenous supply of the electron acceptor decylubiquinone did not improve parasite vitality, as previously shown for asexual atovaquone-inhibited *P. falciparum* parasites (Ke et al., 2011; Figure S6D). Together, these results indicate a stage-dependent regulation of $\Delta\Psi_{mt}$ by PHBL that is independent of the ubiquinone turnover by complex III of the electron transport chain.

DISCUSSION

We show that *Plasmodium* parasites harbor three conserved SPFH proteins and an unusual prohibitin-like protein specific to the Myzozoa. Live-cell imaging of endogenously encoded parasite proteins revealed that the plasmodial SPFH proteins localize to the parasite mitochondrion. Although we could not obtain live localization data for PHB1, the evolutionary conservation of PHB1/2 hetero-oligomerization strongly suggests that *P. berghei* PHB1 is also a mitochondrial protein (Artal-Sanz et al., 2003; Steglich et al., 1999; Nijtmans et al., 2000).

Immunofluorescence analysis using polyclonal antisera directed against a fragment of *P. falciparum* STOML previously suggested localization to the secretory organelles of merozoites and the parasitophorous vacuole during development in erythrocytes (Hiller et al., 2003). This reported localization is at odds with our own observations and computational predictions, which return a 93% probability for mitochondrial import of *P. berghei* STOML (Claros and Vincens, 1996). We fully corroborate the notion by Hiller et al. (2003) that STOML exhibits the most resemblance to stomatin-like protein 2 (SLP2), which was demonstrated to localize to the mitochondria of mice (Da Cruz et al., 2003), humans (Taylor et al., 2003), and plants (Gehl et al., 2014). In addition, our observation of site-specific STOML accumulation during oocyst growth is in agreement with a role in mitochondrial membrane sub-compartmentalization. Together, our data strongly suggest exclusive mitochondrial functions of the SPFH protein family in this single-cell eukaryote.

Gene targeting in *P. berghei* suggests that *PHB1*, *PHB2*, and *STOML* are essential for asexual blood stage development of the parasite. Genetic disruption might cause lethal defects in organellar morphology and segregation, which would be in good agreement with their conserved roles in mitochondrial morphogenesis (Piper et al., 2002; Merkwirth et al., 2008, 2012; Christie et al., 2011). Strikingly, the *PHB1* locus could not be targeted with a non-disruptive tagging construct, most likely because of an interference of the tag with PHB1 protein function. However, the accessibility of the genomic locus, and, thus, the essentiality of PHB1, remain to be formally demonstrated.

Interestingly, *Plasmodium* parasites express an additional and uncommon mitochondrial prohibitin-like SPFH protein, PHBL, specific to the myzozoan clade. In contrast to the *bona fide* PHBs of other organisms, PHBL is expressed at very low levels and not involved in mitochondrial morphogenesis or segregation. Instead, we provide evidence for specific functions of *PHBL* in the regulation of mitochondrial membrane polarity. Several proteins initially thought to aid the generation of $\Delta\Psi_{mt}$, such as complexes I, II, and V of the electron transport chain, were dispensable for $\Delta\Psi_{mt}$ maintenance in transgenic *P. berghei* parasites (Boysen and Matuschewski, 2011; Hino et al., 2012; Sturm et al., 2015). Together with our own observations of normal atovaquone sensitivity and lack of phenotypic rescue by decylubiquinone, these findings lead us to hypothesize that PHBL might regulate membrane polarity independent of individual complexes of the electron transport chain.

The molecular mechanism underlying *PHBL*-dependent depolarization remains to be determined. Mitochondrial SPFH proteins have previously been demonstrated to influence membrane polarity in other systems, which has been linked to impaired sequestration of the respiratory machinery to membrane microdomains (Gehl and Sweetlove, 2014). Similar interactions might be the underlying mechanism behind the *PHBL*-dependent membrane depolarization in malaria parasites.

Whether the lower membrane potential can be attributed to an impairment in the generation of the chemiosmotic gradient or, instead, to its enhanced utilization for ATP production remains to be shown. In most eukaryotic cells, oligomycin inhibition can be used to discriminate between the two potential causes. However, classical ATP synthase inhibitors, like oligomycin or azide, are ineffective in *Plasmodium* (Mather et al., 2010), including in sexual stages, where ookinete formation of WT and *phbl*$^{-}$ parasites was largely unaffected (Figure S7).

Although PHBL is expressed throughout the plasmodial life cycle, we observed the most substantial depolarization of $\Delta\Psi_{mt}$ in sexual stages, culminating in developmental arrest during mosquito midgut colonization. In contrast, *PHBL* appears to be less important for the parasite during infection of the vertebrate host. We note that mitochondrial depolarization during sexual development is not a secondary effect of parasite death because mortality was bypassed by superior growth conditions *in vitro*, suggesting that the degree of depolarization is likely even higher in the mosquito midgut.

The stage-specific arrest caused by the lack of *P. berghei PHBL* is reminiscent of *Saccharomyces cerevisiae PHB1/2*-null mutants. Only non-dividing yeast cells, which are arrested in the stationary G_0 phase, tend to lose respiratory competence (Piper and Bringloe, 2002). It has been argued that this phenomenon might result from an imbalanced turnover of respiratory chain complexes because of the lack of PHBs and insufficient *de novo* synthesis of the respiratory machinery in the resting cell (Piper and Bringloe, 2002). We note that *PHBL*-deficient malaria parasites display a similar developmental specificity for the non-dividing gametocyte and ookinete stages of the life cycle.

Our microscopic quantification shows that the $\Delta\Psi_{mt}$ of WT parasites is most pronounced in macrogametes (~2-fold higher than in trophozoites or ookinetes), suggesting a critical period of enhanced mitochondrial demand during host switching. This is in agreement with previous literature demonstrating an increased dependence on mitochondrial functions during mosquito midgut colonization (Florens et al., 2002; Hall et al., 2005; Srivastava et al., 2016), thus providing a possible explanation for the stage-specific consequences of *PHBL* depletion.

Together, our data demonstrate important mitochondrial functions of the SPFH protein family in malaria parasites and reveal the involvement of an unusual family member in the regulation of $\Delta\Psi_{mt}$ during transmission to the definitive host.

EXPERIMENTAL PROCEDURES

Phylogenetic Reconstruction

See the Supplemental Experimental Procedures for details regarding phylogenetic analysis.

Generation of Recombinant Parasite Lines

We used advanced experimental genetic techniques to generate and isolate all recombinant parasite lines (Janse et al., 2006; Kooij et al., 2012; Kenthirapalan et al., 2012; Matz and Kooij, 2015). Details on vector construction, parasite isolation, and genotyping strategies, including primer sequences and restriction endonuclease recognition sites used for molecular cloning, are provided in Figures 1C, 3A, and S1; Table S1; and Supplemental Experimental Procedures.

Experimental Animals

This study was carried out in strict accordance with the German Tierschutzgesetz in der Fassung vom 22. Juli 2009, the Dutch Experiments on Animals Act (Wod 2014), and the Directive 2010/63/EU of the European Parliament and Council on the Protection of Animals Used for Experimental and Other Scientific purposes. The protocol was approved by the ethics committee of the Berlin state authority (Landesamt für Gesundheit und Soziales Berlin, permit number G0294/15). All animal experiments performed at the Radboudumc were approved by the Radboud University Experimental Animal Ethical Committee (RUDEC 2012-251). Female C57BL/6 mice were used for sporozoite infections and detection of malaria-related complications. All other parasite infections were conducted with male or female NMRI mice.

In Vivo Infections

Asexual blood stage development was assessed using the previously described intravital competition assay (Matz et al., 2013). To test atovaquone sensitivity, highly infected mice received daily intraperitoneal injections of atovaquone (1.44 mg/kg body weight), and parasitemia was measured by flow cytometry. To test transmission efficiency, naive mice were subjected to bites from 100 or more female *A. stephensi* mosquitoes 21 days after the infectious blood meal. Blood stage patency was assessed by either microscopic analysis of Giemsa-stained thin blood films or by flow cytometric analysis of peripheral blood. For details regarding parasite inocula, see the Supplemental Experimental Procedures.

Microscopy

For details regarding fluorescence imaging and electron microscopy, see the Supplemental Experimental Procedures.

Ookinete Cultivation

Ookinetes were cultivated in RPMI 1640 medium (Thermo Fisher Scientific, Waltham, MA, USA) supplemented with 10% fetal calf serum (FCS) (Thermo Fisher Scientific), 50 μM xanthurenic acid, 0.85 g/L $NaHCO_3$ (pH 8.0, ookinete medium), and, in some cases, with varying concentrations of atovaquone, decylubiquinone, or oligomycin A. 10 μL of blood from highly infected mice or the ingested blood from 3 infected mosquitoes was transferred to 90 μL of ookinete medium and incubated in a 96-well plate at 20°C for 24 hr.

Detection of $\Delta\Psi_{mt}$

Rhodamine 123 staining was performed as described previously (Sturm et al., 2015). Asexual blood stage parasites were transferred from infected mice into RPMI 1640 medium supplemented with 20% FCS and stained with 0.1 μg/mL rhodamine 123 for 30 min. In addition, the medium contained either 50 μM of the uncoupling agent FCCP or DMSO as a solvent control. Parasites were washed once in medium and left at 37°C for 30 more min prior to live microscopy. The same procedure was applied to macrogametes and ookinetes, with the alterations that ookinete medium was used and that staining and washing was performed at room temperature.

Statistical Analysis

Most comparisons between two experimental groups were analyzed with a Student's t test. One-way ANOVA in combination with Tukey's multiple comparison test was used for comparisons between more than two groups. Prepatency and development of experimental cerebral malaria were analyzed with a Mantel-Cox test and blood stage development with a two-way ANOVA and linear regression analysis.

SUPPLEMENTAL INFORMATION

Supplemental Information includes Supplemental Experimental Procedures, seven figures, one table, and one video and can be found with this article online at https://doi.org/10.1016/j.celrep.2018.03.088.

ACKNOWLEDGMENTS

We thank Angelika Sturm for expert advice regarding mitochondrial visualization using rhodamine 123. This work was supported by the Max Planck Society, the Humboldt University, the postdoc scholarship program of the Humboldt Graduate School, and the German Research Council through integrated research training program 2290 "Crossing boundaries: molecular interactions in malaria" (GRK2290). J.M.M. and T.W.A.K. are supported by the Netherlands Organization for Scientific Research (NWO-VIDI 864.13.009).

AUTHOR CONTRIBUTIONS

J.M.M., T.W.A.K., and K.M. conceived the study. J.M.M. performed most of the experiments. C.G. prepared and analyzed electron microscopy samples. J.M.M. wrote the manuscript with input from K.M. and T.W.A.K. The final manuscript was edited and approved by all authors.

DECLARATION OF INTERESTS

The authors declare no competing interests.

Received: November 27, 2017
Revised: February 16, 2018
Accepted: March 20, 2018
Published: April 17, 2018

REFERENCES

Artal-Sanz, M., Tsang, W.Y., Willems, E.M., Grivell, L.A., Lemire, B.D., van der Spek, H., and Nijtmans, L.G. (2003). The mitochondrial prohibitin complex is essential for embryonic viability and germline function in *Caenorhabditis elegans*. J. Biol. Chem. *278*, 32091–32099.

Boysen, K.E., and Matuschewski, K. (2011). Arrested oocyst maturation in *Plasmodium* parasites lacking type II NADH:ubiquinone dehydrogenase. J. Biol. Chem. *286*, 32661–32671.

Browman, D.T., Hoegg, M.B., and Robbins, S.M. (2007). The SPFH domain-containing proteins: more than lipid raft markers. Trends Cell Biol. *17*, 394–402.

Christie, D.A., Lemke, C.D., Elias, I.M., Chau, L.A., Kirchhof, M.G., Li, B., Ball, E.H., Dunn, S.D., Hatch, G.M., and Madrenas, J. (2011). Stomatin-like protein 2 binds cardiolipin and regulates mitochondrial biogenesis and function. Mol. Cell. Biol. *31*, 3845–3856.

Claros, M.G., and Vincens, P. (1996). Computational method to predict mitochondrially imported proteins and their targeting sequences. Eur. J. Biochem. *241*, 779–786.

Da Cruz, S., Xenarios, I., Langridge, J., Vilbois, F., Parone, P.A., and Martinou, J.C. (2003). Proteomic analysis of the mouse liver mitochondrial inner membrane. J. Biol. Chem. *278*, 41566–41571.

Florens, L., Washburn, M.P., Raine, J.D., Anthony, R.M., Grainger, M., Haynes, J.D., Moch, J.K., Muster, N., Sacci, J.B., Tabb, D.L., et al. (2002). A proteomic view of the *Plasmodium falciparum* life cycle. Nature *419*, 520–526.

Gehl, B., and Sweetlove, L.J. (2014). Mitochondrial Band-7 family proteins: scaffolds for respiratory chain assembly? Front. Plant Sci. *5*, 141.

Gehl, B., Lee, C.P., Bota, P., Blatt, M.R., and Sweetlove, L.J. (2014). An *Arabidopsis* stomatin-like protein affects mitochondrial respiratory supercomplex organization. Plant Physiol. *164*, 1389–1400.

Hall, N., Karras, M., Raine, J.D., Carlton, J.M., Kooij, T.W., Berriman, M., Florens, L., Janssen, C.S., Pain, A., Christophides, G.K., et al. (2005). A comprehensive survey of the *Plasmodium* life cycle by genomic, transcriptomic, and proteomic analyses. Science *307*, 82–86.

Hiller, N.L., Akompong, T., Morrow, J.S., Holder, A.A., and Haldar, K. (2003). Identification of a stomatin orthologue in vacuoles induced in human erythrocytes by malaria parasites. A role for microbial raft proteins in apicomplexan vacuole biogenesis. J. Biol. Chem. *278*, 48413–48421.

Hinderhofer, M., Walker, C.A., Friemel, A., Stuermer, C.A., Möller, H.M., and Reuter, A. (2009). Evolution of prokaryotic SPFH proteins. BMC Evol. Biol. *9*, 10.

Hino, A., Hirai, M., Tanaka, T.Q., Watanabe, Y., Matsuoka, H., and Kita, K. (2012). Critical roles of the mitochondrial complex II in oocyst formation of rodent malaria parasite *Plasmodium berghei*. J. Biochem. *152*, 259–268.

Janse, C.J., Franke-Fayard, B., Mair, G.R., Ramesar, J., Thiel, C., Engelmann, S., Matuschewski, K., van Gemert, G.J., Sauerwein, R.W., and Waters, A.P. (2006). High efficiency transfection of *Plasmodium berghei* facilitates novel selection procedures. Mol. Biochem. Parasitol. *145*, 60–70.

Kasashima, K., Ohta, E., Kagawa, Y., and Endo, H. (2006). Mitochondrial functions and estrogen receptor-dependent nuclear translocation of pleiotropic human prohibitin 2. J. Biol. Chem. *281*, 36401–36410.

Ke, H., Morrisey, J.M., Ganesan, S.M., Painter, H.J., Mather, M.W., and Vaidya, A.B. (2011). Variation among *Plasmodium falciparum* strains in their reliance on mitochondrial electron transport chain function. Eukaryot. Cell *10*, 1053–1061.

Kenthirapalan, S., Waters, A.P., Matuschewski, K., and Kooij, T.W. (2012). Flow cytometry-assisted rapid isolation of recombinant *Plasmodium berghei* parasites exemplified by functional analysis of aquaglyceroporin. Int. J. Parasitol. *42*, 1185–1192.

Kooij, T.W., Rauch, M.M., and Matuschewski, K. (2012). Expansion of experimental genetics approaches for *Plasmodium berghei* with versatile transfection vectors. Mol. Biochem. Parasitol. *185*, 19–26.

Langhorst, M.F., Reuter, A., and Stuermer, C.A. (2005). Scaffolding microdomains and beyond: the function of reggie/flotillin proteins. Cell. Mol. Life Sci. *62*, 2228–2240.

Mather, M.W., Morrisey, J.M., and Vaidya, A.B. (2010). Hemozoin-free *Plasmodium falciparum* mitochondria for physiological and drug susceptibility studies. Mol. Biochem. Parasitol. *174*, 150–153.

Matz, J.M., and Kooij, T.W. (2015). Towards genome-wide experimental genetics in the *in vivo* malaria model parasite *Plasmodium berghei*. Pathog. Glob. Health *109*, 46–60.

Matz, J.M., Matuschewski, K., and Kooij, T.W. (2013). Two putative protein export regulators promote *Plasmodium* blood stage development *in vivo*. Mol. Biochem. Parasitol. *191*, 44–52.

Merkwirth, C., and Langer, T. (2009). Prohibitin function within mitochondria: essential roles for cell proliferation and cristae morphogenesis. Biochim. Biophys. Acta *1793*, 27–32.

Merkwirth, C., Dargazanli, S., Tatsuta, T., Geimer, S., Löwer, B., Wunderlich, F.T., von Kleist-Retzow, J.C., Waisman, A., Westermann, B., and Langer, T. (2008). Prohibitins control cell proliferation and apoptosis by regulating OPA1-dependent cristae morphogenesis in mitochondria. Genes Dev. *22*, 476–488.

Merkwirth, C., Martinelli, P., Korwitz, A., Morbin, M., Brönneke, H.S., Jordan, S.D., Rugarli, E.I., and Langer, T. (2012). Loss of prohibitin membrane scaffolds impairs mitochondrial architecture and leads to tau hyperphosphorylation and neurodegeneration. PLoS Genet. *8*, e1003021.

Morrow, I.C., and Parton, R.G. (2005). Flotillins and the PHB domain protein family: rafts, worms and anaesthetics. Traffic *6*, 725–740.

Nijtmans, L.G., de Jong, L., Artal Sanz, M., Coates, P.J., Berden, J.A., Back, J.W., Muijsers, A.O., van der Spek, H., and Grivell, L.A. (2000). Prohibitins act as a membrane-bound chaperone for the stabilization of mitochondrial proteins. EMBO J. *19*, 2444–2451.

Osman, C., Merkwirth, C., and Langer, T. (2009). Prohibitins and the functional compartmentalization of mitochondrial membranes. J. Cell Sci. *122*, 3823–3830.

Piper, P.W., and Bringloe, D. (2002). Loss of prohibitins, though it shortens the replicative life span of yeast cells undergoing division, does not shorten the chronological life span of G_0-arrested cells. Mech. Ageing Dev. *123*, 287–295.

Piper, P.W., Jones, G.W., Bringloe, D., Harris, N., MacLean, M., and Mollapour, M. (2002). The shortened replicative life span of prohibitin mutants of yeast appears to be due to defective mitochondrial segregation in old mother cells. Aging Cell *1*, 149–157.

Rivera-Milla, E., Stuermer, C.A., and Málaga-Trillo, E. (2006). Ancient origin of reggie (flotillin), reggie-like, and other lipid-raft proteins: convergent evolution of the SPFH domain. Cell. Mol. Life Sci. *63*, 343–357.

Sinden, R.E., Winger, L., Carter, E.H., Hartley, R.H., Tirawanchai, N., Davies, C.S., Moore, J., and Sluiters, J.F. (1987). Ookinete antigens of *Plasmodium berghei*: a light and electron-microscope immunogold study of expression of the 21 kDa determinant recognized by a transmission-blocking antibody. Proc. R. Soc. Lond. B Biol. Sci. *230*, 443–458.

Srivastava, A., Philip, N., Hughes, K.R., Georgiou, K., MacRae, J.I., Barrett, M.P., Creek, D.J., McConville, M.J., and Waters, A.P. (2016). Stage-specific changes in *Plasmodium* metabolism required for differentiation and adaptation to different host and vector environments. PLoS Pathog. *12*, e1006094.

Steglich, G., Neupert, W., and Langer, T. (1999). Prohibitins regulate membrane protein degradation by the m-AAA protease in mitochondria. Mol. Cell. Biol. *19*, 3435–3442.

Sturm, A., Mollard, V., Cozijnsen, A., Goodman, C.D., and McFadden, G.I. (2015). Mitochondrial ATP synthase is dispensable in blood-stage *Plasmodium berghei* rodent malaria but essential in the mosquito phase. Proc. Natl. Acad. Sci. USA *112*, 10216–10223.

Taylor, S.W., Fahy, E., Zhang, B., Glenn, G.M., Warnock, D.E., Wiley, S., Murphy, A.N., Gaucher, S.P., Capaldi, R.A., Gibson, B.W., and Ghosh, S.S. (2003). Characterization of the human heart mitochondrial proteome. Nat. Biotechnol. *21*, 281–286.

van Dooren, G.G., Marti, M., Tonkin, C.J., Stimmler, L.M., Cowman, A.F., and McFadden, G.I. (2005). Development of the endoplasmic reticulum, mitochondrion and apicoplast during the asexual life cycle of *Plasmodium falciparum*. Mol. Microbiol. *57*, 405–419.